Patient-specific generation of the Purkinje network driven by clinical measurements of a normal propagation

Christian Vergara · Simone Palamara · Domenico Catanzariti · Fabio Nobile · Elena Faggiano · Cesarino Pangrazzi · Maurizio Centonze · Massimiliano Maines · Alfio Quarteroni · Giuseppe Vergara

Received: 1 July 2013 / Accepted: 8 August 2014

C. Vergara (✉)
Dipartimento di Ingegneria, Università di Bergamo,
Viale Marconi 5, 24044 Dalmine, BG, Italy
e-mail: christian.vergara@unibg.it

S. Palamara · F. Nobile · E. Faggiano · A. Quarteroni
MOX, Dipartimento di Matematica, Politecnico di Milano,
Piazza Leonardo da Vinci 32, 20131 Milan, Italy

D. Catanzariti · C. Pangrazzi · M. Maines · G. Vergara
Divisione di Cardiologia, Ospedale S. Maria del Carmine,
Corso Verona, 4, 38068 Rovereto, TN, Italy

F. Nobile · A. Quarteroni
MATHICSE-CSQI, École Polytechnique Fédérale de Lausanne,
SB SMA-GE, MA B2 444 (Bâtiment MA), Station 8,
1015 Lausanne, Switzerland

E. Faggiano
LaBS, Dipartimento di Chimica, Materiali e Ingegneria
Chimica, Politecnico di Milano, Piazza Leonardo da Vinci 32,
20131 Milan, Italy

M. Centonze
U.O. di Radiologia di Borgo-Pergine, Viale Vicenza 9,
38051 Borgo Valsugana, TN, Italy

Abbreviations

PF	Purkinje fibers
CCS	Cardiac conduction system
PMJ	Purkinje muscular junctions
MRI	Magnetic resonance imaging
3D	Three dimensional
AV	Atrioventricular
ECG	Electrocardiogram

1 Introduction

The Purkinje fibers (PF) represent the peripheral part of the cardiac conduction system (CCS) and are located just beneath the endocardium. Their main role consists in

providing rapid and coordinate activation of the ventricular myocardium [9], an essential feature for the correct pumping of the blood flow into the arteries. PF are electrically connected to the ventricular muscle only at certain insertion sites, called Purkinje muscle junctions (PMJ) [19]. From these sites, the depolarization wave enters the ventricle muscle, allowing the ventricular excitation and contraction [2].

The mathematical and computational models of cardiac electrophysiology allow to compute virtually the electrical activity in the ventricles [13]. The inclusion of CCS and in particular of the PF in such models is therefore essential to simulate the ventricular activation. While the anatomical reconstruction of the heart geometry is possible thanks to the modern imaging techniques (such as MRI and CT), radiological images do not allow to identify and reconstruct the PF. For this reason, the inclusion of the PF in the computational models has been obtained so far either by means of surrogates such as the definition of space-dependent conduction properties [25], or by means of the automatic generation of the Purkinje network based on an a priori anatomical knowledge [1, 11, 23]. In the first case, no explicit representations of the Purkinje network have been included in the computation, whereas in the second case no patient-specific models have been generated.

In this work, we propose a method for the generation of a *patient-specific* Purkinje network driven by clinical measures of the activation times on the endocardium of the left ventricle during a normal propagation, thus overcoming the limitations of the techniques previously described. This method is valid only when data on the endocardium related to a normal propagation are used and it is very appealing since it requires to solve differential problems only on the endocardium, thus avoiding the reconstruction of the muscular fibers in the myocardium and the coupling with the torso. At the best of the authors' knowledge, this is the first attempt to use clinical data for the explicit construction of the PF by means of computational models.

2 Methods

2.1 Patient-specific clinical measurements

2.1.1 Acquisition of imaging data and reconstruction of the endocardium geometry

We considered three subjects characterized by a normal electrical propagation. Firstly, they underwent magnetic resonance imaging (MRI). Using a 1.5-Tesla MRI Unit (Magnetom Avanto, Siemens Medical Systems, Erlangen, Germany) and a eight-channel phased-array torso coil, a non-contrast enhanced three-dimensional (3D) whole-heart sequence, cardiac and respiratory gated, was performed using the following parameters: voxel resolution of $1.7 \times 1.6 \times 1.3$ mm; TR (repetition Time) = 269.46 ms; TE (EchoTime) = 1.46 ms; flip angle = 90°; slice thickness = 1.3 mm with 104 slices per single slab; acquisition matrix = 256×173.

Then, the segmented images of the left ventricle endocardium have been obtained by processing the MRI study using the EnSite Verismo™ Segmentation Tool (EnSite Verismo 2.0.1), which is based on a threshold method. Later, the segmented images have been used to build the computational domains in view of the numerical simulations and have been imported into the EnSite NavX system to acquire the activation times. In particular, the number of vertices in the endocardial meshes was 189,274 points for subject 1, 172,290 for subject 2 and 571,382 for subject 3.

2.1.2 Acquisition of electrical data

The activation time in a point is defined as the time difference between a selected fiducial point on the body surface electrocardiogram (ECG) and the steepest negative intrinsic deflection in the unipolar intracardiac electrogram recorded from the tip of a mapping catheter, signifying that the activation front has reached the subjacent muscle. The Ensite NavX system is capable of accurately locating any electrode catheter within a 3D navigation field, allowing the reconstruction of the geometry of any cardiac chamber and providing accurate, real-time catheter navigation to guide mapping of the activation times. In particular, the mapping catheters could be moved along a chamber's surface to record local endocardial electrogram amplitudes, while simultaneously recording location points to generate a 3D geometry of the chamber. NavX system allows to simultaneously display multiple catheter positions in real time. The system consists of three pairs of patches placed on the body surface in orthogonal axes. A low-power 5.7-kHz electrical potential is generated across each pair of patches, and the voltage gradient from each axis generates the three-dimensional navigation field. Based on this, the system measures the local voltage of any electrode that is placed within the navigation field, and thus accurately measures the related electrical activation time. The EnSite NavX technology provides an algorithm for compensation of catheter shifts due to respiratory motion. It is based on the identification of breathing-dependent changes of transthoracic impedances. The current version of digital image fusion function of the EnSite NavX system allowed the segmented endocardium to be displayed side by side and synchronously rotated with the constructed geometry. As for the accuracy of this system, we mention [22], where the authors showed through in vivo experiments that this system enables accurate and reproducible real-time localization of electrode

positions with a precision of 0.7 ± 1.5 mm, and [31], where the application of this system has been showed to not distort the quality of the local ECG. For further details on the EnSite NavX system, we refer the reader to [4, 10]. We observe that this procedure is not repeatable, in the sense that another acquisition would lead to different acquisition points.

In our cases, for all the three subjects, the left ventricular mapping has been performed in the context of a bi-ventricular mapping. To this aim, a 7-Fr deflectable electro-catheter has been inserted through the right femoral artery with a retrograde trans-aortic approach (Medtronic Enhancr II 5523/Medtronic Conductr). All these subjects were characterized by a normal electrical propagation. In particular, we acquired the measures in 186 points for subject 1, in 156 points for subject 2 and in 284 points for subject 3.

2.2 Patient-specific generation of the Purkinje fibers network

The normal electrical activity of the left ventricle is characterized by a front propagating through the Purkinje network and then within the ventricle muscle. In particular, in the normal propagation, the front starts from the atrioventricular (AV) node and propagates in the proximal part of the PF with a velocity in the range 3–4 m/s [15]. At the mid-anteroseptal level, located on the endocardium, the PF start to be connected with the ventricular muscle cells through the PMJ. In this way, the electrical signal enters the ventricle muscle and propagates in the whole myocardium, with a reduced conduction velocity in the range 0.3–0.8 m/s [15].

2.2.1 General overview of the algorithm

The starting point of our method is the use of a fractal law to generate a *tentative* Purkinje network as proposed in [1, 11, 23]. Then, such a network is corrected using the data of the normal activation acquired with the EnSite NavX system, allowing to obtain a patient-specific network. In particular, our method can be summarized in the following steps:

Generation of the patient-specific Purkinje network using data of a normal propagation and computation of the activation times in the left ventricle:

1. Manually design of the bundle of His and of the main bundle branches;
2. Generation of a *tentative* Purkinje network without using the clinical data;
3. Computation of the activation times in the tentative network and in particular at the PMJ;
4. Computation of the activation times on the endocardium of the left ventricle using as input the activation times at the tentative PMJ computed at step 3;
5. Comparison between the activation times computed at step 4 and the measured data;
6. Generation of the *patient-specific* Purkinje network as a correction of the tentative one, driven by the discrepancies between the computed and the measured data obtained at step 5;
7. Computation of the activation times in the patient-specific network and in particular at the PMJ;
8. Computation of the activation times in the endocardium (or in whole left ventricle) using as input the activation times at PMJ computed at step 7.

We notice that the algorithm for the patient-specific Purkinje network generation involves only steps from 1 to 6. Here, we have added also steps 7 and 8 for the computation of activation times in the endocardium or even in the whole left ventricle, since this was the final goal of the PF generation. We also observe that at steps 3–4 and 7–8 we firstly solved the network solely (steps 3, 7), and then, we used this solution evaluated at the PMJ as sources for the computation of the muscular activation (steps 4, 8). This is an *explicit* solution strategy, since it does not account for the feedback of the muscular activation on the Purkinje network. This choice was justified by the fact that for a normal electrical activity the propagation in the PF is not influenced by the muscular propagation (see also [24]).

2.2.2 Modeling the electrical activity

We illustrate now the mathematical models used to compute the activation times (steps 3, 4, 7 and 8 in our algorithm). One of the most widely used models for the description of the electrical activity in the myocardium is the so-called *bidomain equation,* obtained by considering a propagation both in the extra- and in the intra-cellular spaces [8, 14, 30]. However, if one is interested only in the activation times, then the simpler Eikonal equation could be considered [6, 12]. This is a steady model that allows to recover for any point of the computational domain the time at which the potential reaches the value $(W_r + W_p)/2$, where W_r is the minimum of the potential and W_p the value reached at the plateau. This simple model has been often used for clinical applications, see, for example, the recent work [28].

As observed, the patient-specific clinical data were available only on the endocardium. For this reason, in view of the comparison between computed and measured data at step 5 of our algorithm, we needed to know the computed activation times on such a surface. Then, we decided to consider the mathematical model for the electrical propagation only on the endocardium (and not in the whole myocardium) given by the *isotropic* version of the Eikonal model, which reads

$$V_e|\nabla u_e| = 1 \quad \mathbf{x} \in \Omega_e,$$
$$u_e(x) = u_{e,0}(x) \quad \mathbf{x} \in \Gamma_e \tag{1}$$

where $u_e(\mathbf{x})$ is the unknown activation time at a point of the endocardium with coordinates $\mathbf{x}$, Ω_e is the computational domain representing the endocardium, Γ_e is the set of points generating the front, that is, the PMJ, $u_{e,0}(\mathbf{x})$ is the value of the activation times in Γ_e, and V_e is the velocity of the front, tuned in the range 0.3–0.8 m/s maximizing the agreement with the clinical measures. We observe that Ω_e is a surface, so that the gradient has to be intended as the projection of the gradient onto the tangential plane at $\mathbf{x}$.

For the solution of Eq. (1) at step 4 of the algorithm, one needs to know the source term $u_{e,0}$ that represents the activation times at the PMJ. To obtain such values, the activation times in the Purkinje tentative network must be known (steps 3). Analogously, to compute the final electrical activity (step 8), one needs to know the activation times in the patient-specific network to provide the source terms to Eq. (1) (step 7). Therefore, we needed to introduce a mathematical model to compute the activation times also in a Purkinje network. With this aim, we considered again an isotropic Eikonal model, more precisely

$$V_p\left|\partial u_p/\partial s\right| = 1 \quad \mathbf{x} \in \Omega_p,$$
$$u_p(x) = u_{p,0}(x) \quad \mathbf{x} \in \Gamma_p \tag{2}$$

where $u_p(\mathbf{x})$ is the unknown activation time at the point of the network with coordinates $\mathbf{x}$, Ω_p is the computational domain representing the network, Γ_p is set of points generating the front (in the normal propagation the AV node), $u_{p,0}(\mathbf{x})$ represents the activation times in Γ_p, and V_p is the velocity of the front, supposed to be constant and tuned in the range 3–4 m/s, maximizing the agreement with the clinical measures. We observe that the computational domain Ω_p in this case is a line, so that the derivatives have to be intended as directed along the tangent s.

For the numerical solution of the Eikonal Eqs. (1) and (2), we considered the fast marching method [26], implemented in the software VMTK (www.vmtk.org).

2.2.3 *Details of the patient-specific generation of the Purkinje network*

We provide here a few details of the algorithm described above.

2.2.3.1 Generation of a tentative network At step 1, the bundle of His and the main bundle branches were manually designed, according to anatomical a priori knowledge [1, 23]. At step 2, a tentative network as a fractal tree was generated. The growing process followed the 'Y' production rule, similar to the one implemented in [1, 11, 23]. In our approach, at each level of the generation, we identified *active branches* and *leaves*. An active branch can generate other branches, whereas the leaves terminate at their end points which are identified with the PMJ. In this way, the branches could be characterized by a different number of levels. To ensure a correct distribution of the PMJ on the endocardium, we described the process of generation of a leaf by means of a Bernoullian probability, where the probability to generate a leaf, p, is a function of the tree level. In particular, we have

$$p = \sqrt{\frac{j}{M}}$$

where j is the current level and M is the maximum number of levels, so that p is small for the first levels and grows up for the successive levels. To obtain a more realistic pattern of PF, we described the lengths L_l and L_r and the branching angle α of the new fibers by means of Gaussian variables, with mean value 4.0 ± 0.3 mm for the lengths and $60 \pm 1.8°$ for the angle [22], see Fig. 1.

The active branches stopped to generate new branches when one or more of the following conditions were satisfied:

1. The active branches intersected other branches;
2. The active branches reached the zone identified either with the basis or with the upper areas of the mid-antero septum (these regions being not reached by the Purkinje network [24]);
3. The maximum number of levels M defined by the user has been reached.

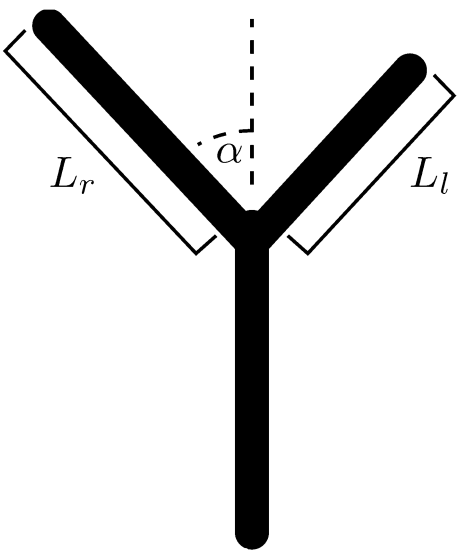

Fig. 1 Schematic representation of the generation of two new branches in the Purkinje network. L_l, L_r and α indicate Gaussian variables

This algorithm produces a front of active branches which propagates and eventually reaches all the regions of the endocardium covered by the Purkinje fibers (formed by all the endocardium apart from the basis and the upper part of the septum). Since the length of the branches is always described by a Gaussian law with the same mean and standard deviation, we noticed that after a finite number of levels the density of leaves per unit area does not change anymore in the regions already reached by the front. Thus, the number of levels of the tree M was determined for each patient with a trial-and-error procedure so that the front has reached all the regions of interest.

The procedure described above allowed to generate a network which in what follows has been referred to as *tentative network*.

2.2.3.2 Computation of the discrepancy between measured and computed data The activation times on the PMJ were then computed by solving the 1D Eikonal Eq. (2) in the tentative network (step 3). These activation times were then used as sources for the Eikonal problem (1) on the endocardium (step 4), allowing to obtain a tentative activation map which was then compared with the experimental data (step 5).

2.2.3.3 Generation of the patient-specific network The algorithm passed then to the final stage, represented by step 6 and consisting in adapting the tentative network to the clinical data using the discrepancies computed at step 5. Accordingly, the leaves of the network were moved or deleted in order to satisfy the data. This is a completely new step with respect to previous works in the generation of PF and allowed to obtain a patient-specific Purkinje network. In particular, for each point $\boldsymbol{x}_j$ where the measures were available, we defined its *region of influence* as the set S_j of PMJ which were possible sources determining the activation time t_j in $\boldsymbol{x}_j$ when solving the 2D Eikonal Eq. (1). In other words, PMJ not belonging to S_j did not contribute in determining the solution in $\boldsymbol{x}_j$. To obtain such regions, we proceeded as follows:

(a) We solved a 2D *backward* Eikonal problem using the measures in $\boldsymbol{x}_j$ as sources;
(b) Given a PMJ P_i located in $\boldsymbol{y}_i$, we concluded that P_i belonged to S_j if it has been activated at step (a) by the source located in $\boldsymbol{x}_j$.

This allowed to associate to any PMJ P_i an activation time τ, solution of the backward problem, which is nothing but the boundary condition which would guarantee that P_i activates the point $\boldsymbol{x}_j$ at time t_j (see Fig. 2a). We then compared the activation time τ in P_i obtained by solving the backward problem with τ_i obtained by solving the 1D Eikonal problem in the network. If these two values were in agreement (in our case, we considered a threshold equal to 15 %), we concluded that PMJ P_i is able to activate the measure located in $\boldsymbol{x}_j$ and then P_i does not need to be moved or deleted. Otherwise, we moved P_i in order to minimize the mismatch between τ and τ_i (see Fig. 2b). In particular, we located P_i on the line joining the base Z_i of the leaf with the measure located in $\boldsymbol{x}_j$ and we looked for the position which guarantees, among all the points on such

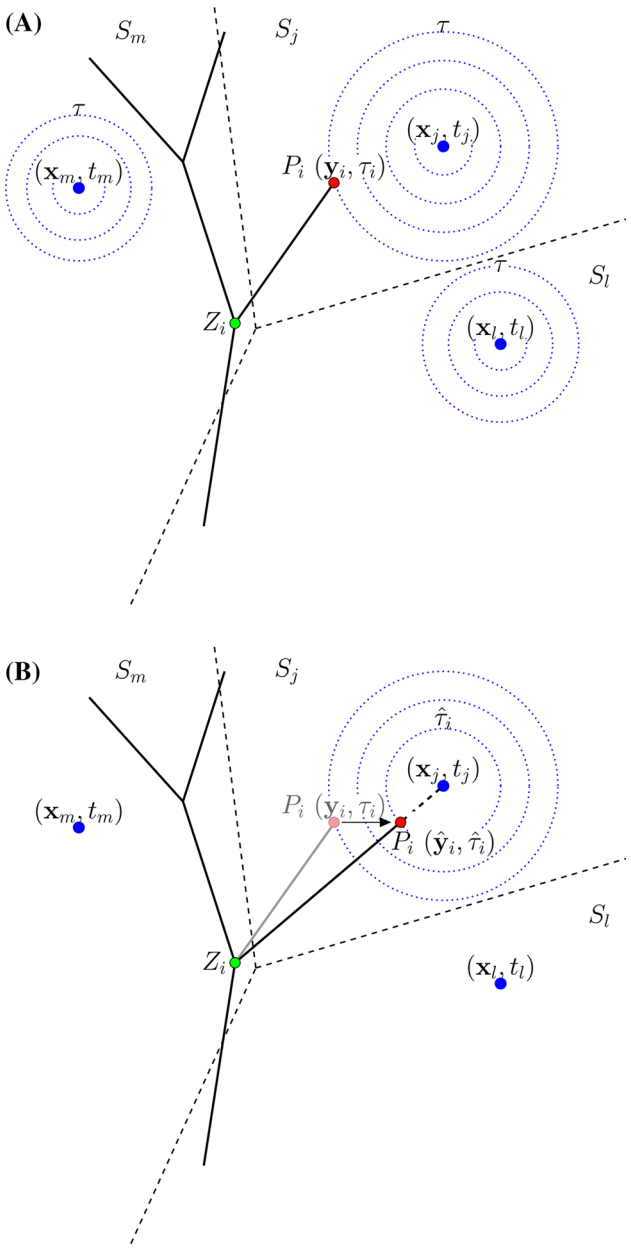

Fig. 2 **a** The first backward signal reaching PMJ P_i starts from measure x_j so that P_i belongs to the region of influence S_j; **b** PMJ P_i is then moved in order to maximize the accordance between the activation time τ_i computed by the network and that predicted by the backward Eikonal solution τ

a line, the best accordance (*moving procedure*). If none of such points allowed to obtain a discrepancy less than 15 %, we then deleted the PMJ P_i and the related leaf (*delete procedure*). If some of the points are not yet satisfied, we created new leaves so to satisfy all the data (*create procedure*). All the details of the algorithm can be found in [17].

We observe that the value of the threshold is a user parameter that can be tuned to improve the accuracy of the algorithm. In our case, we have used a trial-and-error strategy.

Finally, we notice that the network generated by the method depends on the starting tentative network, which is randomly generated with Bernoullian and Gaussian variables, and on some user parameters such as the mean value of the length and of the angles of the branches, the threshold to detect the satisfied points, and the conduction velocities. Once the tentative network and these parameters have been fixed, the solution produced by our algorithm after the moving and delete procedures is unique, in the sense that it generates always the same network. However, the create procedure produces different networks depending on the order used to investigate the not satisfied points.

The code for the implementation of this algorithm has been written in C++ using the VTK 5.8 library.

2.3 Models for a computational comparison

In order to assess the accuracy of the numerical solutions obtained with our strategy (referred in what follows to as model D), we compared its performance with the one of other three scenarios used so far in the literature:

1. Model A. This is the most common model considered so far in the literature when neither the Purkinje network nor clinical measurements were available. In particular, the source for problem (1) is located in a single point at the apex of the ventricle. This strategy does not reproduce accurately the physiology (remember that the electrical signal enters in the ventricle at the level of the mid-antero septum). However, it has been widely used by several authors (see, e.g., [20]) as a simple surrogate to replicate the physiological conditions using only a single source. For a visualization of such a model, see the subfigures at the top/left in Fig. 3;
2. Model B. This model has been considered so far when no Purkinje network is available, whereas measures of the activation times are known. In particular, in this case, the localization of the sources for problem (1) is driven by the measures and the idea is to identify such sources with the points with the smallest measured activation times. This allows to obtain a patient-specific model, see, e.g., [25]. For a visualization of such a model, see subfigures at the top/right in Fig. 3;
3. Model C. This model has been considered so far when a Purkinje network has been generated but no clinical measures are available. The generation of the network is often driven by a fractal law. The idea is to solve an Eikonal or a bidomain problem in the network and then to use the activation times at the PMJ as sources for problem (1), see, e.g., [1, 11, 23].
4. Model D. It is the new model proposed in this work consisting in the generation of a patient-specific network. In particular, we used a part of the data to generate such a network and the remaining part to validate it (cross-validation). For this reason, we divided the measures in two sets: the *training set* composed by 50 % of the measures for the generation of the patient-specific network and the *testing set* composed by the remaining 50 % of the measures for the validation. We notice that also models A, B and C have been validated using the same testing set.

3 Results

In this section, we show the numerical results related to the normal propagation of the three subjects, referred in what follows to as subjects 1, 2 and 3. The goal is to compare the measured activation times with those computed by the four scenarios described above. Given a point on the endocardium where a measure was available, we say that the related datum has been *satisfied* (up to tolerance *tol*) by one of the four models if the relative difference in activation time between the datum and the computed value was less than *tol*. We observed that the ratio of the performance among different models was rather constant with respect to *tol* (however, not lower than the threshold used in the algorithm). We report here the results obtained by setting $tol = 15$ %, thus equal to the threshold used in the algorithm.

Our starting points were, for each of the three subjects, the geometries reconstructed from the MRI data and the measured activation times. Since we have used a probabilistic model to generate the Purkinje tentative network, each run of our method produced a different outcome. For this reason, we ran the algorithm 20 times for each subject, generating 20 tentative and 20 patient-specific networks. In Table 1, first two rows, we reported the mean number of branches and PMJ in the generated networks. In Fig. 3, for each of the subjects, at the top we indicated the localization of the sources for models A and B, whereas at the bottom we reported a selected network generated by our algorithm for models C and D.

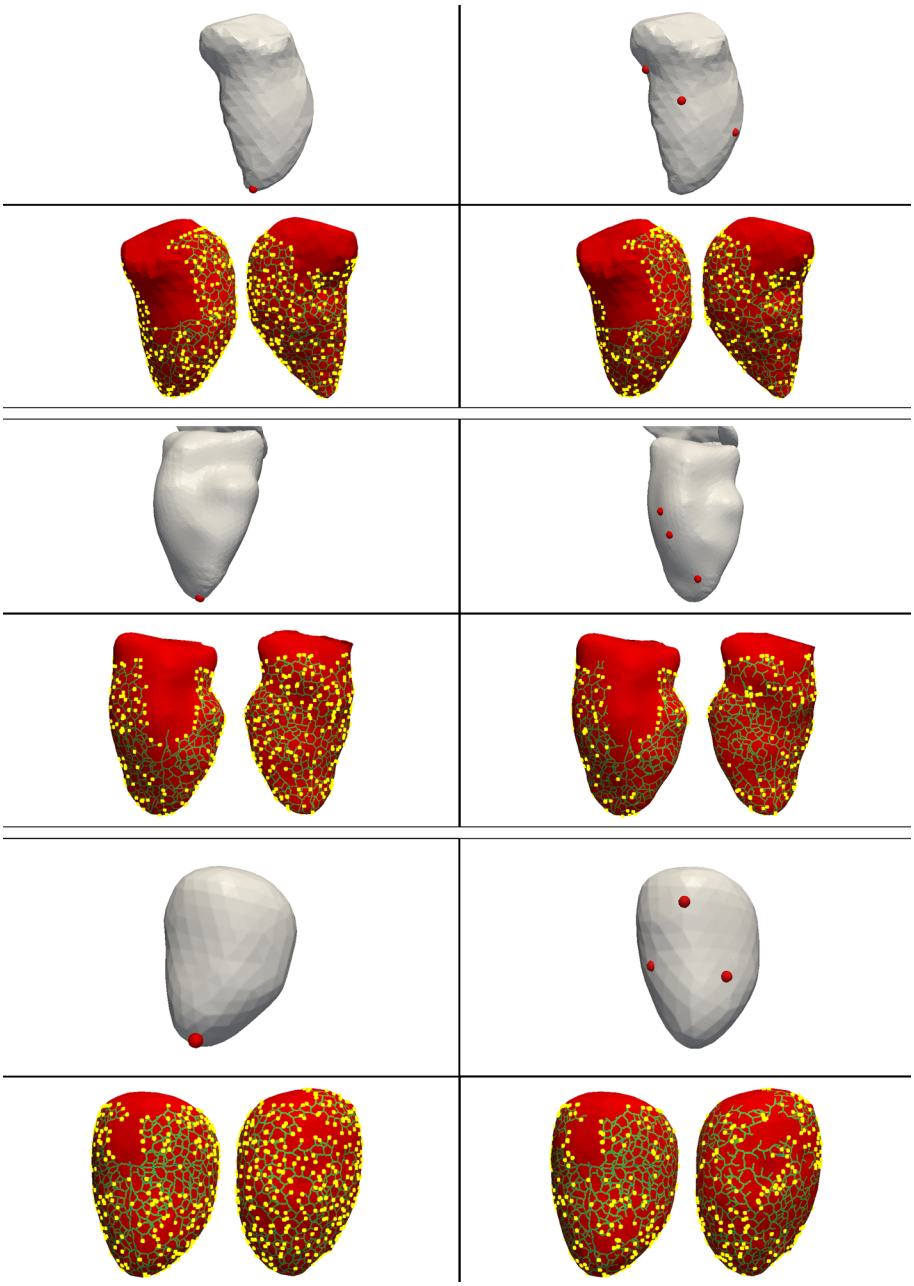

Fig. 3 Subjects 1, 2 and 3. *Top* Localization of the sources in the models without PF: Model A (*left*) and model B (*right*). *Bottom* Tentative (model C, *left*) and patient specific (model D, *right*) Purkinje networks generated by our algorithm. The *yellow bullets* represent the PMJ. For models C and D, we depicted one selected case over the 20 simulated (color figure online)

Once we have identified for each model the sources for the 2D problem, we solved the Eikonal problem (1) on the endocardium, obtaining the activation times for all the four models, reported in Figs. 4, 5 and 6. For models C and D, we depicted one selected case over the 20 simulated. The velocities of conduction in the network (V_p) and on the endocardium (V_e) have been tuned in order to maximize the number of satisfied points and have been kept constant over the 20 simulations for models C and D. We reported such quantities in Table 1, third and fourth rows. We observe that for models C and D such values fell into the physiological ranges (3–4 m/s for V_p and 0.3–0.8 m/s for V_e). Regarding models A and B, the absence of the PF network has been supplied by choosing a conduction velocity V_e which could change over the domain [25]. In particular, we chose two different values of such a velocity, one in the region of the endocardium activated by the PF and another one in the region characterized by a purely muscular activation (that is, at the base of the ventricle and at the upper areas of the mid-antero septum). From Table 1, we observe that for models A and B we let V_e assume values outside the muscular physiological range (but consistent with the conduction velocity in the network) to account for the PF propagation.

In Figs. 4, 5 and 6, we plotted also the measured activation times (represented with squares) and the absolute error

Table 1 Number of branches and of PMJ of the networks generated by models C and D, and estimated conduction velocities in the network (V_p) and on the endocardium (V_e)

	Model A	Model B	Model C	Model D
Subject 1				
# Branches	X	X	1,946 ± 74	1,735 ± 72
# PMJ	X	X	474 ± 24	311 ± 21
V_p (m/s)	X	X	3.9	3.9
V_e (m/s)	3.8/0.8	3.1/0.8	0.6	0.6
Subject 2				
# Branches	X	X	1,515 ± 54	1,439 ± 51
# PMJ	X	X	337 ± 15	261 ± 13
V_p (m/s)	X	X	3.9	3.9
V_e (m/s)	2.8/0.8	2.1/0.8	0.6	0.6
Subject 3				
# Branches	X	X	2,529 ± 73	2,430 ± 68
# PMJ	X	X	608 ± 29	253 ± 12
V_p (m/s)	X	X	3.2	3.2
V_e (m/s)	2.2/0.8	2.1/0.7	0.4	0.4

For V_e in models A and B, the first value refers to the endocardium excluding the base of the ventricle and the upper areas of the mid-antero septum, while the second one refers to the base of the ventricle and the upper areas of the mid-antero septum. For models C and D, the results have to be intended as the average over the 20 simulations

(that is the distance between computed and measured data) at each point. We observe an excellent qualitative agreement between measured and computed data obtained with our method, whereas a comparable accuracy was obtained by models B and C. Model A seemed to feature the poorest accuracy among the four models.

In order to quantify the accuracy of the different models, we computed the percentage of satisfied points and the average absolute error in activation time between the measures and the prediction by the four models in each measurement point. We reported such values in Table 2, which confirmed the better accuracy of the model with a patient-specific Purkinje network (model D) with respect to the other ones.

As for the computational time needed to run our method for the generation of the patient-specific network and the computation of the activation times, we typically had a CPU time of about 350 s for each run, split into the different steps of the algorithm as follows:

- Generation of the tentative network (step 2): 65 %;
- Solution of the 1D and 2D Eikonal problems (steps 3 and 4): 5 %;
- Correction to generate the patient-specific network (step 6): 25 %;
- Final solution of the 1D and 2D Eikonal problems (steps 7 and 8): 5 %.

From these results, we observe that the generation of the patient-specific network requires a little extra time with respect to the generation of the tentative one.

4 Discussion

4.1 State of the art

Mathematical models of the cardiac electrophysiology allow to compute virtually the electrical activity in the ventricles, providing a non-invasive tool for the study of the propagation of the electrical signal [13]. Despite PF have an essential function in the coordinated activation of the ventricles, they have been usually neglected in the computational models. This was mainly due to the difficulty in obtaining in vivo images of the PF, which are excessively thin for the current clinical imaging resolution.

A common strategy used so far to obtain significant results without generating explicitly the Purkinje network consisted in locating the source of the front at the apex of ventricle (model A) [20]. An alternative approach has been considered in [25], where the sources were localized by analyzing available clinical data and defining space-dependent conduction properties (model B). Nevertheless, accounting for the PF in ventricular computational models is essential to simulate the normal activation [21, 29]. For this reason, some scientists have attempted to incorporate PF in the mathematical models by their explicit construction. Three possible alternatives have been proposed so far:

1. A manual procedure based on the anatomical knowledge [3, 29];
2. The segmentation of PF from ex vivo images [5];
3. The construction of the Purkinje network computationally with a semiautomatic algorithm [1, 11, 23].

In the latter case, the network generation was driven by general anatomical information and thus was not patient specific (model C). In this work, we proposed to use the same approach, where, however, *the construction of PF has been driven by clinical patient-specific data* concerning the activation times on the endocardium during a normal propagation (model D). At the best of our knowledge, this has been the first attempt to use clinical data for the explicit construction of the Purkinje network by means of computational tools, *allowing to obtain patient-specific networks*.

4.2 Discussion of the results

We applied models A, B, C and D to three subjects characterized by a normal conduction activity (see Figs. 3, 4, 5, 6;

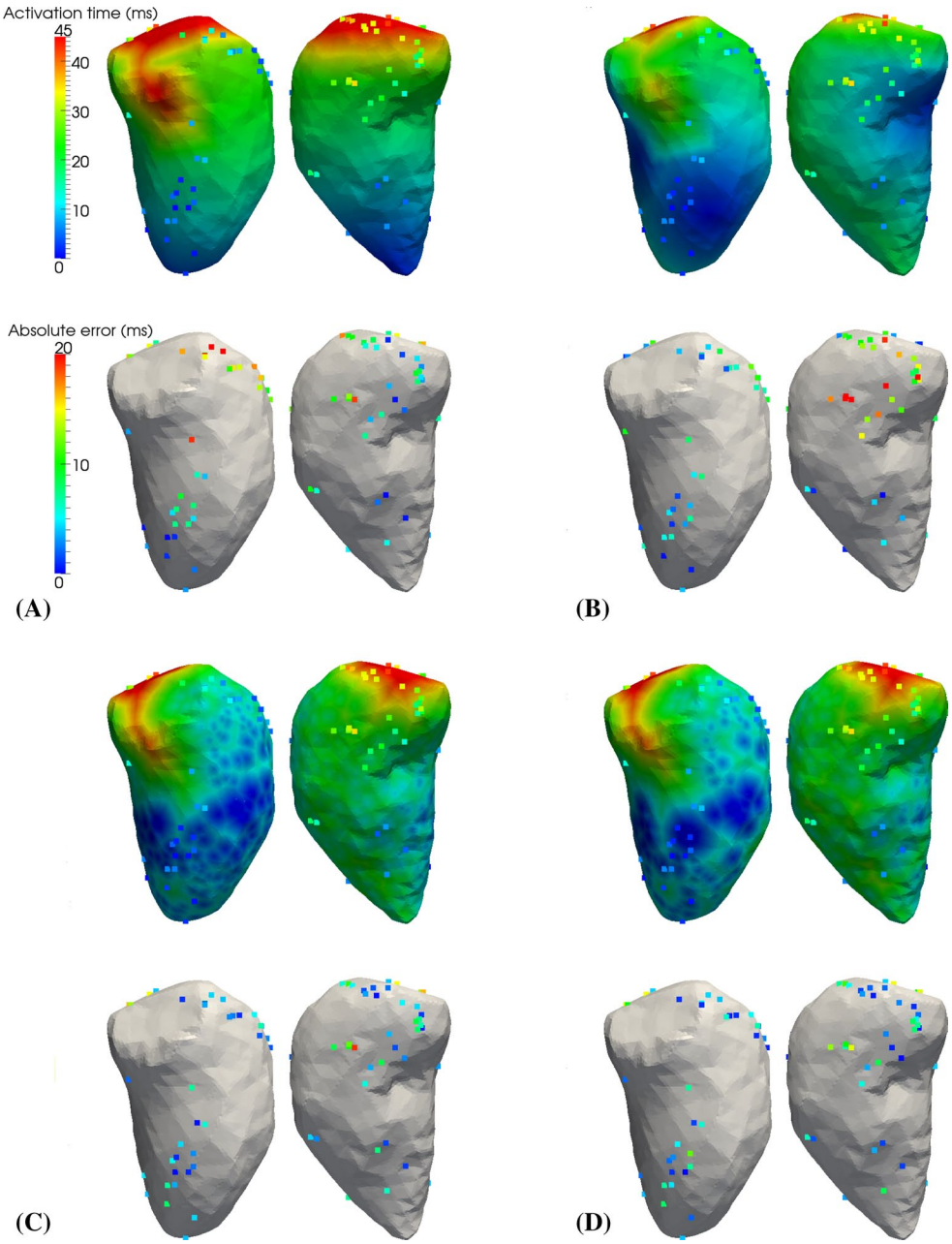

Fig. 4 Computed activation times and absolute errors for the four models. *Top left*, model A. *Top right*, model B. *Bottom left*, model C. *Bottom right*, model D. For each case, in the *upper row* we depicted the computed activation times (the measured data are plotted with *squares*) and in the *lower row* we represented the absolute errors. For models C and D, we depicted one selected case over the 20 simulated. Subject 1, normal activation (color figure online)

Tables 1, 2). We divided the measures in the training set for the generation of the patient-specific network in model D and in the testing set for the validation of all the four models. Each of these two groups was composed by 50 % of the total points (cross-validation test).

The numerical results showed that the absolute errors obtained with model B decreased in the three subjects by 4, 22 and 32 %, respectively, in comparisons of the ones obtained with model A, while the number of satisfied points increased by 6 % for subject 3 and decreased for subjects 1 and 2. This showed that the use of clinical data allowed to improve the accuracy of the numerical results when no PF were modeled, at least for what concerns the absolute error. We also noticed that the values of the mean absolute error and of the standard deviation obtained with model B are in good accordance with those obtained in [25].

The same conclusion concerning the importance of using clinical data to improve the accuracy was obtained also for the models with a Purkinje network. Indeed, the absolute errors related to model D decreased in the three subjects by 9, 19 and 25 %, respectively, in comparisons of the ones obtained with model C, while the number of satisfied points increased by 6, 31 and 53 %, respectively.

By comparing the performance obtained by models which exploited clinical measures (models B and D),

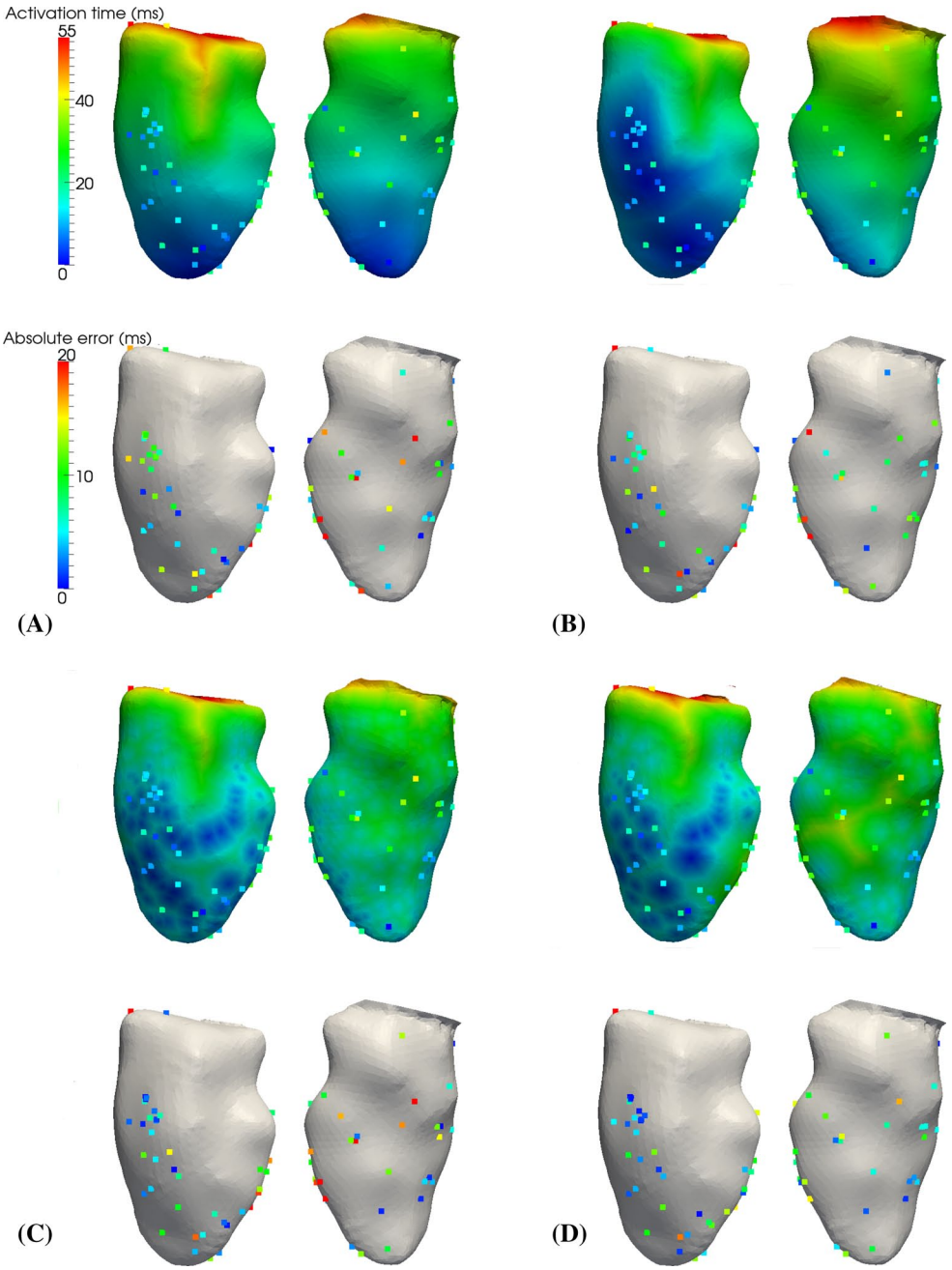

Fig. 5 Computed activation times and absolute errors for the four models. *Top left*, model A. *Top right*, model B. *Bottom left*, model C. *Bottom right*, model D. For each case, in the *upper row* we depicted the computed activation times (the measured data are plotted with *squares*) and in the *lower row* we represented the absolute errors. For models C and D, we depicted one selected case over the 20 simulated. Subject 2, normal activation (color figure online)

we found that the inclusion of the Purkinje network is fundamental to obtain accurate results. Indeed, the absolute errors obtained with model D decreased in the three subjects by 40, 23 and 17 %, respectively, in comparisons of the ones obtained with model B, while the number of satisfied points increased by 92, 214 and 29 %, respectively.

From these results, we observed that by performing a cross-validation test there was a clear improvement in the performance of model D with respect to the other models. In particular, the mean absolute error was lower in all the cases with respect to that featured by the other models. Analogously, model D featured the highest number of satisfied points.

By comparing the accuracy of models B and C, we found that such methods featured more or less the same accuracy. This showed that using the clinical data without modeling the Purkinje network or modeling the network without using the clinical data brought more or less to the same level of accuracy.

All these facts clearly showed the importance of using both clinical data and a patient-specific Purkinje network to obtain accurate results by numerical simulations of a normal propagation.

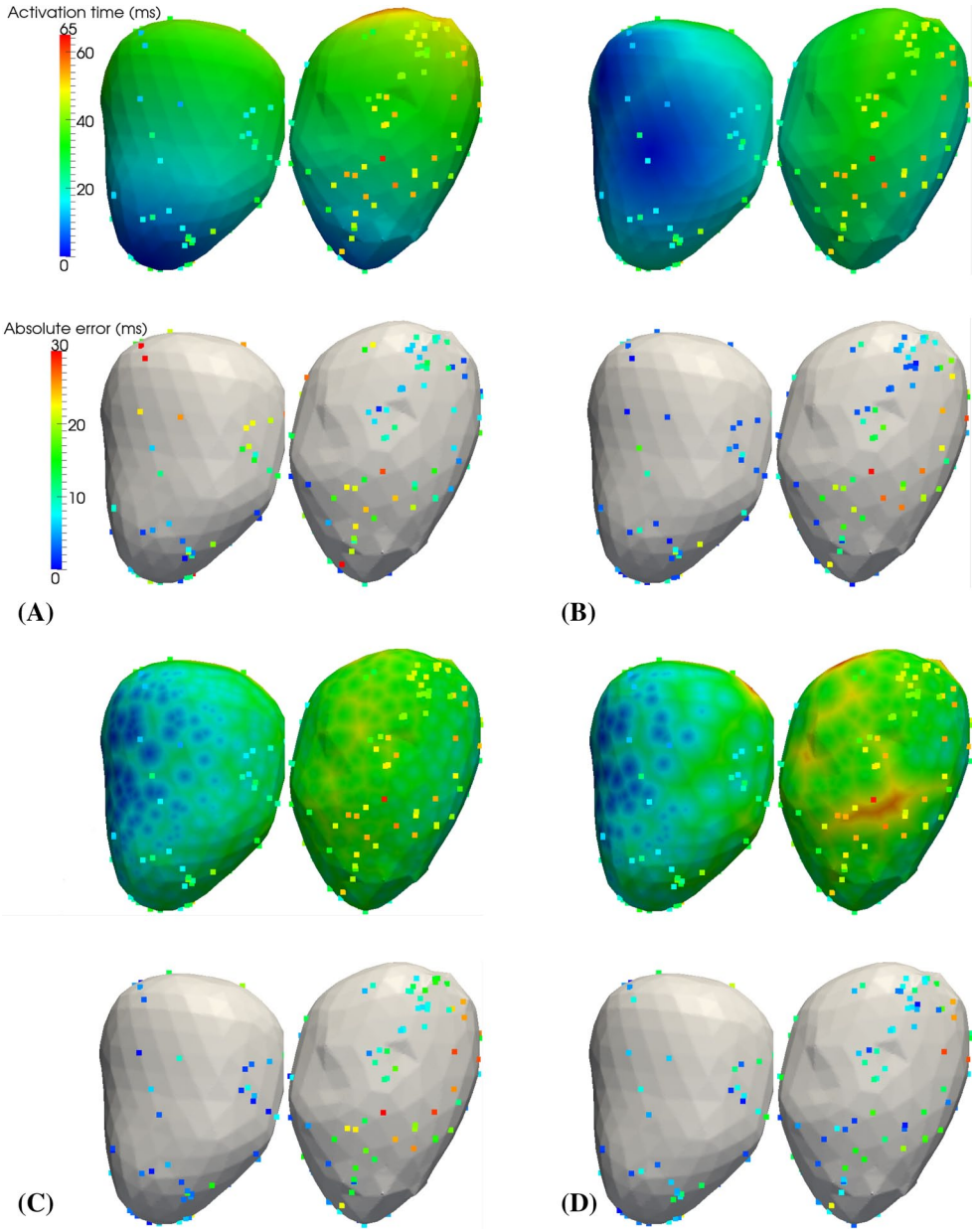

Fig. 6 Computed activation times and absolute errors for the four scenarios. *Top left*, model A. *Top right*, model B. *Bottom left*, model C. *Bottom right*, model D. For each case, in the *upper row* we depicted the computed activation times (the measured data are plotted with *squares*), while in the *lower row* we represented the absolute errors. For models C and D, we depicted one selected case over the 20 simulated. Subject 3, normal activation (color figure online)

4.3 On the variability patient to patient

Here, we want to study whether the mean error obtained with our model is comparable with the variability of the measures patient to patient. If this was the case, then the extra effort to do patient-specific network may be unnecessary. Otherwise, the construction of a patient-specific Purkinje network would be justified and its accuracy would not be given by the fortuity.

To obtain the variability patient to patient, we computed the mean values of the activation measures for each patient and then the standard deviation σ among the three mean values. We found $\sigma = 9.25$ ms, which is in any case greater than the mean absolute errors obtained with model D, see Table 2, last column. This highlighted that the extra effort needed to build a patient-specific network is perfectly justified in terms of an improvement of the accuracy.

4.4 On the sensitivity of the accuracy on the number of measures

From the results reported in Table 2, we observed that the accuracy of model D is quite sensitive to the number of measures, in particular the percentage of satisfied points increased for an increasing number of measures. These observations lead to the (quite expected) conclusion that by increasing the number of available measures, the accuracy

Table 2 Percentage of satisfied points (that is, characterized by an error less than 15 %) and mean absolute error for the three cases in the four models

	Satisfied points (%)	Mean absolute error (ms)
Subject 1		
Model A	23.8	8.4 ± 5.7
Model B	19.2	8.1 ± 6.2
Model C	34.6 ± 5.8	5.4 ± 4.5
Model D	36.8 ± 4.7	4.9 ± 4.1
Subject 2		
Model A	16.7	10.2 ± 7.8
Model B	11.1	8.0 ± 6.3
Model C	26.6 ± 3.8	8.0 ± 6.8
Model D	34.8 ± 2.8	6.5 ± 5.4
Subject 3		
Model A	27.9	13.1 ± 10.2
Model B	29.5	8.9 ± 7.5
Model C	25.0 ± 3.7	9.9 ± 7.5
Model D	38.2 ± 3.7	7.4 ± 6.6

For models C and D, the results have to be intended as the average over the 20 simulations. Cross-validation with 50 % of the points used to generate the network in model D and the remaining 50 % to validate all the models

of the results obtained when using the patient-specific Purkinje network increased.

4.5 On the validity of the proposed model

In this work, we considered the activation times related to a normal ventricle propagation. In such a condition, it is possible to exploit two assumptions concerning the electrical propagation:

- The electrical signal propagates firstly on the endocardium and then into the myocardium starting uniquely from the PMJ;
- There is no feedback of the muscular activation on the Purkinje network.

These assumptions are supported by [27], which highlighted that in the presence of an active Purkinje network and for an endocardial source, no returning fronts could activate the endocardium. These two assumptions lead to great simplifications in the model to generate a patient-specific Purkinje network. Indeed, on the one hand, the propagation in the myocardium does not influence that on the endocardium and therefore at step 4 of our algorithm is enough to solve a problem only on the endocardium. On the other hand, since the propagation in the Purkinje network is not influenced by the muscular propagation, the choice of using an explicit algorithm to solve the coupled electrical network/muscle problem is perfectly justified, leading to a simple algorithm which does not need to introduce subiterations (see also [24]).

As observed, our method is valid only when data on the endocardium related to a normal propagation are considered. In the case of a pathological propagation, the two assumptions above are not still valid in general, so that one needs to account for the muscular fibers (and then for the anisotropy) and for an implicit algorithm to manage the electrical coupling between the network and the muscle. The extension of our model to the pathological case can be found in [16].

4.6 On the choice of using the Eikonal model

Regarding the mathematical models used to compute the activation times [problems (1) and (2)], we considered in this work the Eikonal equation both for the PF and for the endocardium. In its more complex version, this model accounts for the orientation of the muscular fibers and for the diffusion process characterizing the front (anisotropic Eikonal-diffusion equation [18, 25]). This model was proved to be a good approximation of the more complex bidomain one for computing the activation maps in the myocardium [7] and has been recently considered also for clinical applications [28].

In this work, we made two approximations for the Eikonal equation. On the one hand, we considered the isotropic version of such a model. This could be justified by noticing that, for a normal activation, the signal enters the ventricle at the level of the endocardium, propagating first on such a surface and then in the myocardium, and that in the presence of an active Purkinje network no returning fronts could activate the endocardium [27]. Therefore, for a normal ventricle activation, the propagation on the endocardium is not influenced by the myocardial muscular fibers that are located downstream, along the thickness of the myocardium. Despite the presence of muscular fibers also on the endocardium, which influence the electrical propagation on this surface [27], we assumed that the solution on the endocardium is mostly determined by the Purkinje fibers, in particular by the PMJ, which are so dense to attenuate any anisotropic phenomenon on the endocardium. These facts motivated our choice of using the isotropic equation. However, this approximation represents a limitation of this study, and 2D (or even 3D) anisotropic models will be considered in future works to improve the accuracy of the method. On the other hand, we neglected the diffusion term, since we assumed that the diffusion process gives a small contribution with respect to the advection one. This was justified by noticing that PF were so dense to inhibit the diffusion to become relevant.

Concerning the propagation in the PF, these two approximations (isotropy and absence of diffusion) were perfectly justified, due to the absence of fibers (and then of anisotropy) in the network, and to the high advection term V_p which dominated any diffusion process.

4.7 Possible extension to non-invasive data

The method proposed in this work was presented for data related to the activation times on the endocardium acquired with the NavX system. To acquire such data, an invasive procedure is needed based on the implantation of catheters in the left ventricle. Often, such invasive data are not available, so that we ask whether our method could be applied to non-invasive data as well. For example, electrocardiographic signals in the torso could be used to generate a patient-specific network. In this case, at step 5 of the algorithm, one needs to compute the ECG signals on the torso starting from the Eikonal solution in the ventricle and to compare them with the data. Of course, we expect to obtain a more accurate network when using invasive data, since ECG data on the torso give a poorer information, being surrogates of the activation times in the ventricle.

5 Conclusions

In this work, we proposed a method for the computation of a patient-specific Purkinje network starting from clinical measurements of a normal electrical propagation, to be used to improve the computational models for the computation of the electrical activity in the left ventricle. The main contributions of the present work are summarized in what follows:

- We showed, for the first time, the feasibility of using clinical measurements of the activation times on the endocardium to drive the Purkinje network generation by means of computational tools, allowing to recover patient-specific networks;
- We showed an improvement of the accuracy in the case of a normal propagation when patient-specific measures were used to drive the simulation, both in the absence and in the presence of a Purkinje network;
- We showed the importance of generating a patient-specific Purkinje network to recover an accurate electrical activation on the endocardium for a normal propagation, when clinical measures are available;
- We showed that the solution of the simple isotropic Eikonal model solved only on the endocardium was enough to generate accurate patient-specific Purkinje networks.

These conclusions showed that the proposed method is able to provide an effective tool to improve the accuracy in the computation of the normal electrical activity of the left ventricle. The next step we are working on is the extension of such a method to the description of pathological cases such as Wolff–Parkinson–White [16].

Acknowledgments The present study has been funded by Fondazione Cassa di Risparmio di Trento e Rovereto (CARITRO) within the project "Numerical modelling of the electrical activity of the heart for the study of the ventricular dyssynchrony". The authors would like also to acknowledge St. Jude Medical Inc. and in particular Eng Indiani for their helpful assistance for the description of the technical characteristics of the NavX system.

Conflict of interest We state that there are no disclosures.

References

1. Abboud S, Berenfeld O, Sadeh D (1991) Simulation of high-resolution QRS complex using a ventricular model with a fractal conduction system. Effects of ischemia on high-frequency QRS potentials. Circ Res 68(6):1751–1760
2. Anderson RH, Yanni J, Boyett MR, Chandler NJ, Dobrzynski H (2009) The anatomy of the cardiac conduction system. Clin Anat 22(1):99–113
3. Berenfeld O, Jalife J (1998) Purkinje-muscle reentry as a mechanism of polymorphic ventricular arrhythmias in a 3-dimensional model of the ventricles. Circ Res 82(10):1063–1077
4. Bhakta D, Miller JM (2008) Principles of electroanatomic mapping. Indian Pacing Electrophysiol J 8(1):32–50
5. Bordas R, Gillow K, Lou Q, Efimov IR, Gavaghan D, Kohl P, Grau V, Rodriguez B (2011) Rabbit-specific ventricular model of cardiac electrophysiological function including specialized conduction system. Prog Biophys Mol Biol 107(1):90–100
6. Colli Franzone P, Guerri L (1993) Spreading excitation in 3-D models of the anisotropic cardiac tissue, I. Validation of the Eikonal model. Math Biosci 113:145–209
7. Colli Franzone P, Guerri L, Pennacchio M, Taccardi B (1998) Spread of excitation in 3-d models of the anisotropic cardiac tissue. II. Effects of fiber architecture and ventricular geometry. Math Biosci 147(2):131–171
8. Colli Franzone P, Pavarino LF (2004) A parallel solver for reaction–diffusion systems in computational electrocardiology. Math Models Methods Appl 14(06):883–911
9. Durrer D, van Dam RR, Freud GE, Janse MJ, Meijler FL, Arzbaecher RC (1970) Total excitation of the isolated human heart. Circulation 41(6):899–912
10. Eitel C, Hindricks G, Dagres N, Sommer P, Piorkowski C (2010) EnSite Velocity™ cardiac mapping system: a new platform for 3D mapping of cardiac arrhythmias. Expert Rev Med Devices 7(2):185–192
11. Ijiri T, Ashihara T, Yamaguchi T, Takayama K, Igarashi T, Shimada T, Namba T, Haraguchi R, Nakazawa K (2008) A procedural method for modeling the Purkinje fibers of the heart. J Physiol Sci 58(7):481–486
12. Keener JP (1991) An Eikonal-curvature equation for action potential propagation in myocardium. J Math Biol 29(7):629–651
13. Keener JP, Sneyd J (1998) Mathematical Physiology. Springer, New York
14. Keener JP, Bogar K (1998) A numerical method for the solution of the bidomain equations in cardiac tissue. Chaos 8(1):234–241

15. Kerckhoffs RC, Faris OP, Bovendeerd PH, Prinzen FW, Smits K, Arts T (2003) Timing of depolarization and contraction in the paced canine left ventricle: model and experiment. J Cardiovasc Electr 14(10 Suppl):S188–S195
16. Palamara S, Vergara C, Catanzariti D, Faggiano E, Centonze M, Pangrazzi C, Maines M, Quarteroni A (2014) Patient-specific generation of the Purkinje network driven by clinical measurements: the case of pathological propagations. MOX Report n. 4/2014
17. Palamara S, Vergara C, Faggiano E, Nobile F (2013) An effective algorithm for the generation of patient-specific Purkinje networks in computational electrocardiology. MOX Report n. 48/2013
18. Pashaei A, Romero D, Sebastian R, Camara O, Frangi A (2011) Fast multiscale modeling of cardiac electrophysiology including purkinje system. IEEE T Biomed Eng 58(10):2956–2960
19. Rawling DA, Joyner RW, Overholt ED (1985) Variations in the functional electrical coupling between the subendocardial purkinje and ventricular layers of the canine left ventricle. Circ Res 57(2):252–261
20. Rodriguez B, Li L, Eason JC, Efimov IR, Trayanova NA (2005) Differences between left and right ventricular chamber geometry affect cardiac vulnerability to electric shocks. Circ Res 97(2):168–175
21. Romero D, Sebastian R, Bijnens B, Zimmerman V, Boyle P, Vigmond E, Frangi A (2010) Effects of the Purkinje system and cardiac geometry on biventricular pacing: a model study. Ann Biomed Eng 38:1388–1398
22. Rotter M, Takahashi Y, Sanders P, Haïssaguerre M, Jaïs P, Hsu LF, Sacher F, Pasquié JL, Clementy J, Hocini M (2005) Reduction of fluoroscopy exposure and procedure duration during ablation of atrial fibrillation using a novel anatomical navigation system. Eur Heart J 26(14):1415–1421
23. Sebastian R, Zimmerman V, Romero D, Frangi A (2011) Construction of a computational anatomical model of the peripheral cardiac conduction system. IEEE T Biomed Eng 58(12):3479–3482
24. Sebastian R, Zimmerman V, Romero D, Sanchez-Quintana D, Frangi A (2012) Characterization and modeling of the peripheral cardiac conduction system. IEEE T Med Imaging 32(1):45–55
25. Sermesant M, Chabiniok R, Chinchapatnam P, Mansi T, Billet F, Moireau P, Peyrat JM, Wong K, Relan J, Rhode K, Ginks M, Lambiase P, Delingette H, Sorine M, Rinaldi CA, Chapelle D, Razavi R, Ayache N (2012) Patient-specific electromechanical models of the heart for the prediction of pacing acute effects in CRT: a preliminary clinical validation. Med Image Anal 16(1):201–215
26. Sethian JA (1999) Level set methods and fast marching methods: evolving interfaces in computational geometry, fluid mechanics, computer vision, and materials science. Cambridge University Press, Cambridge
27. Taccardi B, Lux RL, Ershler PR, MacLeod R, Dustman TJ, Ingebrigtsen N (1997) Anatomical architecture and electrical activity of the heart. Acta Cardiol 52(2):91–105
28. Tobon-Gomez C, Duchateau N, Sebastian R, Marchesseau S, Camara O, Donal E, De Craene M, Pashaei A, Relan J, Steghofer M, Lamata P, Delingette H, Duckett S, Garreau M, Hernandez A, Rhode KS, Sermesant M, Ayache N, Leclercq C, Razavi R, Smith NP, Frangi AF (2013) Understanding the mechanisms amenable to CRT response: from pre-operative multimodal image data to patient-specific computational models. Med Biol Eng Comput. doi:10.1007/s11517-013-1044-7
29. Tusscher KH, Panfilov AV (2008) Modelling of the ventricular conduction system. Prog Biophys Mol Biol 96(1–3):152–170
30. Vigmond EJ, Aguel F, Trayanova NA (2002) Computational techniques for solving the bidomain equations in three dimensions. IEEE Trans Biomed Eng 49(11):1260–1269
31. Wittkampf FH, Wever EF, Derksen R, Wilde AAM, Ramanna H, Hauer RNW, Robles de Medina EO (1999) LocaLisa: new technique for real-time 3-dimensional localization of regular intracardiac electrodes. Circulation 99(10):1312–1317